PINSA, **67, A,** No. 4 & 5, July & September 2001, pp. 509-529.
© Printed in India.

LIGHTNING EFFECTS IN MESOSPHERE AND ASSOCIATED ELF RADIO SIGNALS

M HAYAKAWA* AND A P NICKOLAENKO+

* *Department of Electronic Engineering, The University of Electro-Communications, Chofu, Tokyo (Japan)*

+ *Usikov Institute for Radio Physics and Electronics of the Ukrainian National Academy of Sciences, Kharkov (Ukraine)*

(Received 03 November 1999; Accepted 01 May 2000)

We demonstrate that an extension of vertical cloud-to-ground lightning magnifies its ELF radiation. We use a multiple bent stroke model of vertical discharge. Motion of the current wave combined with bending of the lightning channel results in multiple pulses radiated into atmosphere that may cause bunching and focusing of the free charged particles of the middle atmosphere. The pulses are unobservable at the ground or right above the stroke. To detect them, the airborne measurements should be performed at some tens km distance from the discharge and at as high altitude as possible. We also demonstrate that repetitious electromagnetic pulses originating from multiple bent strokes turn into a single pulse when propagating in the Earth-ionosphere cavity. A remote observer detects a single pulse and cannot distinguish between ELF transients arriving from a single extremely energetic vertical discharge and from the staircase stroke.

Key Words: Lightning; ELF Waves; Mesosphere

1 Introduction

Two topics played an important role in the atmospheric electricity during the last decade. One of these was connected with the documented discovery of luminous structures in the atmosphere that accompany lightning strokes and appear above powerful thunderstorms. These optical phenomena were classified as red sprites, blue jets, elves[1,2]. We mention below the main features of optical events. Detailed information and extended references may be found in the papers[1-9], in the special issue of the *Journal of Atmospheric and Solar-Terrestrial Physics*, **60**, No. 7-9, 1998 and in *Proceedings of 11th International Conference on Atmospheric Electricity*, Guntersville, Alabama, June 7-11, 1999, Marshall Space Flight Center, Alabama, 1999.

Heating of the electrons in the lower ionosphere by electromagnetic radiation of vertical lightning stroke was analyzed in ref. [10]. Similar problem for the horizontal discharge was treated in ref. [11], and an improved model was developed in ref. [12]. These works treated the heating by moderate lightning discharges. The paper by Inan *et al.*[13] considered heating of the lower ionosphere by lightning to explain absorption and phase changes of VLF radio signals. Optical emissions caused by electromagnetic (EM) waves in the lower ionosphere were analyzed in Taranenko *et al.*[14]. A substantial progress had been achieved in interpreting and modelling of experimental data recently (see, e.g., the special issue of the Journal of *Atmospheric and Solar-Terrestrial Physics*, **60**, No. 7-9, 1998).

The second popular item was the link between world-wide thunderstorm activity and global warming. The physical idea was expressed by Williams[15] in a following way. Ground temperature drives the atmospheric convection. Increase in convection accelerates the cloud formation, charge separation and production of thunderstorm cells. Lightning activity is the main source for the global electromagnetic (or Schumann) resonance that occurs in the cavity between the Earth and ionosphere at frequencies 8, 14, 20, 26 *Hz* etc.. Thus, the amplitude of the Schumann resonance signal becomes a global thermometer. The advantage of such an approach lies in a possibility to measure the median global temperature from a single remote observatory because SR is a global phenomenon.

Natural electromagnetic radiation in the SR frequency band that extends from a few Hz to some

tens of Hz is a superposition of continuous background noise and discrete intense pulses. The transient pulses may exceed the level of regular continuous background by a factor of ten[16-18]. Transient pulses are called Q-bursts when measured at SR frequencies, they are regarded as slow tail atmospherics when detected at frequencies higher than a few hundred *Hz*. Such signals originate from 'super lightning strokes' that occur approximately once per minute. An advantage of transient signals is based on possibility to solve the inverse electromagnetic problem, i.e., to find the coordinates and current moment of the causative stroke[17,18-20].

A link had been discovered recently between the optical phenomena and these transient signals of extremely low frequency (ELF) band[8,21,22].

The main idea of the present paper is based on the fact that the strokes causing optical events eventually produce substantial electromagnetic radiation concentrated in the lower part of the ELF band, at frequencies below a few hundred *Hz*. Relevant radio waves are able to circle multiply the globe due to small attenuation. Hence, an energetic lightning stroke associated with the optical event may simultaneously launch an ELF radio wave into the Earth-ionosphere duct. The Q-burst signal could be used for remote sensing of the lightning discharge, and finding appropriate coordinates and characteristics. Application of such a technique showed that ELF transients are associated with positive lightning discharges causing the red sprites[8,21,22].

In the present paper, we demonstrate that many features of electromagnetic and optical events appear in the framework of rather simple and convincing model of multiple bent lightning strokes. Actually, this is the classical return stroke model with modified geometry. We show that geometry of the lightning channel and finite velocity of current wave in it determine temporal and spectral characteristics of the EM fields. We compute electric fields of the model strokes in neutral atmosphere either in the vicinity of the source or at a far-away distance. The results so obtained clarify basic properties of both optical phenomena and of discrete ELF radio signals.

2 Optical Phenomena

The main portion of optical phenomena was observed and documented in the U.S. from the Yucca Ridge Field Station (40° 40' N and 104° 56' W)[3]. Observations are combined with the concurrent information from National Lightning Detection Network (NLDN). Hence, the coordinates, peak current and polarity of the parent strokes are known. Recently, independent ground based observations of the red sprites were reported in other parts of the world[23,24].

A few words should be said about setup of optical and ELF radio wave ground-based observatories.

The Yucca Ridge Field Station looms above the western edge of American middle west plains[3,4]. It offers ideal conditions for observing thunderstorms over this great territory. Intense mesoscale convective systems (MSCS) are formed over plains in summer producing intense night thunderstorms. The typical distance from the site to the lightning strokes is around five-six hundred kilometers. Therefore, the cloud tops are hidden under the horizon, and a sensitive video camera is able to record relatively weak optical phenomena above the MSCS. To conduct such observations, one needs a territory where MSCS are formed with great lightning activity at night, a remote elevated place to install optical equipment, and no optical sources along the line of vision. At present time, the work is underway to find such an isolated place in Japan allowing for the sky monitoring during winter thunderstorm activity over Japan sea. An appropriate place had been already found in Australia[23]. We think that similar observations are possible in other parts of the world as well. A detailed description of optical measurements is given in Lyons[3].

An ELF file-site is placed in the rural area, and it records the natural radio signals arriving from the global thunderstorm activity[8,9,16,17,20,21,25-27]. EM waves are detected by vertical electric and two orthogonal horizontal magnetic ferrite core antennas. Industrial interference at 50 (60) *Hz* and harmonics are a serious obstacle for measurements. As a rule, the ELF receiver reduces the industrial signal by 50-60 *dB*, and its typical bandwidth is 4-40 *Hz*. The vertical electric antenna is sensitive to local weather conditions, and the normal work of magnetic antennas may be distorted by vibrations (therefore, they are buried in the ground).

Measurements of slow tail atmospherics are made at frequencies above 300 *Hz*. These are much easier to perform because interference in both electric and magnetic components decrease with frequency. Unfortunately, round-the-world radio propagation

(and, hence, the global resonance) is impossible in this band.

The ELF hardware output is usually fed to a personal computer via analog-digital-converter (ADC) board. The data accumulation and preliminary processing is carried out by a special software. More detailed description of equipment is given in the literature[8,9,16,17,20,21,25-27].

Fig. 1 presents a diagram of optical events connected with electric activity in the atmosphere. Red sprites typically occupy the altitude range from 55 to 90 km. They consist as a rule of a few filaments and a 'cloudy' cover, their upper part carries a 'plume.' The typical duration is some tens of milliseconds. Elves are observed between 75 and 95 *km* altitudes, and are fast transient events (less than 1 *ms*) caused by the heating of the lower ionosphere by EM pulse radiated from the lightning discharge. Blue jets and blue starters (the latter ones are shorter) are extended from the cloud top, i.e., 15-20 *km* to 40 (jets) or 25 *km* (starters). Two former events always follow the strokes of lightning, while the latter phenomena may occur without distinct parent stroke.

3 Various Stroke Models

3.1 Basic Model of the Return Stroke

We consider electric fields produced by the median return stroke of lightning[28]. There is an extensive literature on the lightning discharges[29]. However, the publications containing analytical models of the lightning strokes remain relatively rare. Besides, practically all the works model the vertical return strokes of lightning[30,31]. Since the pioneer work of

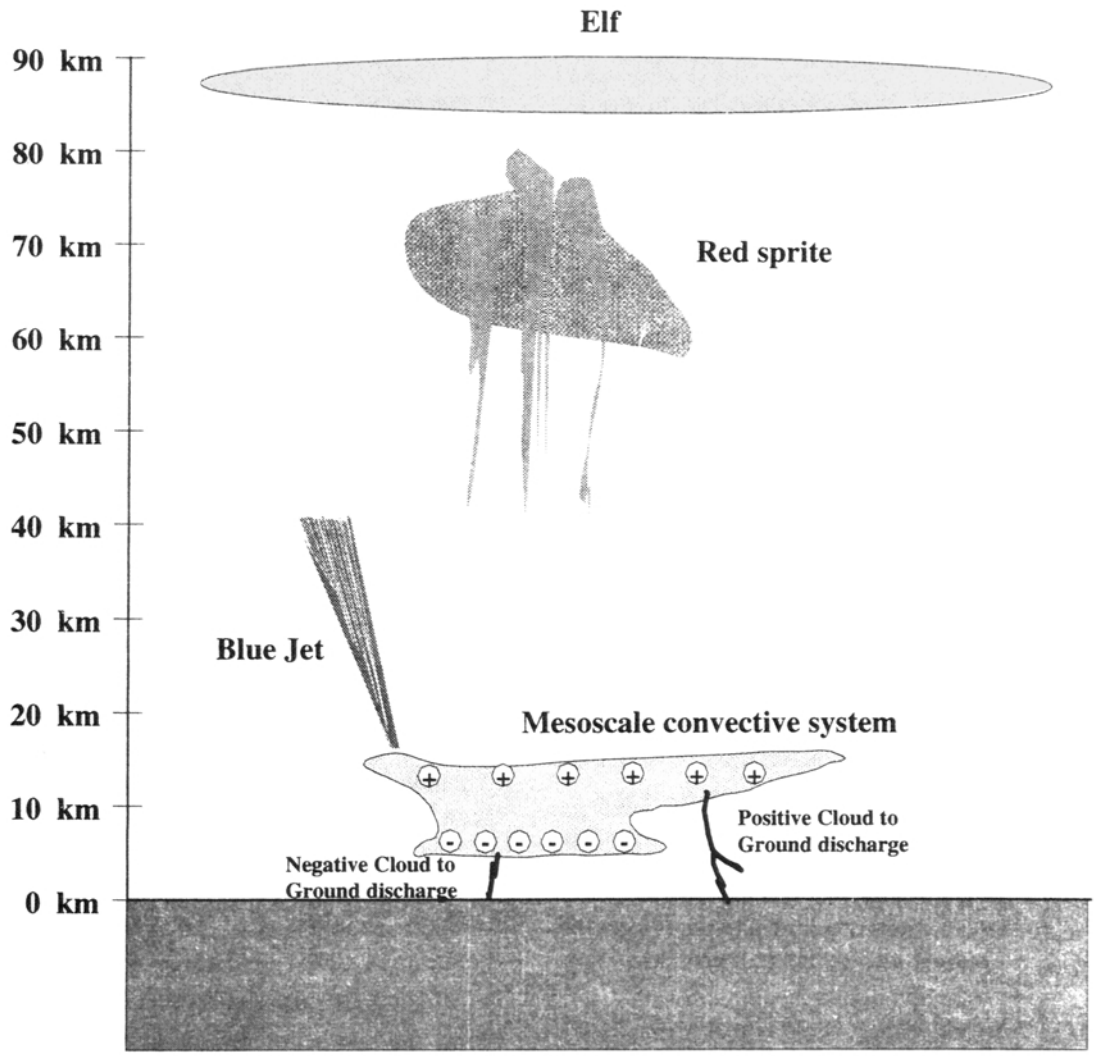

Fig. 1 Schematics of lightning strokes and optical events in the atmosphere

Bruce and Golde[32], the current at the base of such a stroke is described as a sum of exponential terms (two terms were introduced originally). Difference between the models lies in the number of terms (up to four), their amplitudes and decay factors. These parameters are found within the same order of magnitude for all the models. We had chosen the appropriate model[28] since it accounts for intermediate and continuing currents of the stroke via introducing third and fourth terms in the current.

The current of the return stroke begins at $t = 0$. It is introduced at the ground base of the discharge as the sum of four exponential terms:

$$I(t)=\begin{cases} 0 & \text{when } t < 0 \\ \sum_{k=1}^{4} I_k \exp\{-\omega_k t\} & \text{when } t \geq 0 \end{cases} \quad \ldots (1)$$

Here, I_k is the amplitude of individual term, and ω_k is relevant inverse time constants of the current. Table I specifies the values we use throughout the work. The parameters are typical for an engineering model of the return stroke[33].

Table I

Parameters of the currents in the basic model of return stroke.

k	Currents I_k kA	Time constants of the currents τ_k s	Characteristic frequency $\omega_k = 1/\tau_k$ s^{-1}
1	-28.45	1.66×10^{-6}	6.0×10^{5}
2	23.0	3.33×10^{-5}	3.0×10^{4}
3	5.0	5.0×10^{-4}	2.0×10^{3}
4	0.450	6.8×10^{-3}	147.0

The last term in eq. (1) describes the continuing current of 450 *A*. It is responsible for the final decay of the electrostatic field of the stroke. Combination of four terms in the current waveform provides the peak current of $I_p(t) \cong 24\ kA$ reached at $t=5.5\ \mu s$, and an exponential decay occurs afterwards. Positive current in a return stroke is directed upward since the cloud bottom carries a negative charge. It transfers the negative electric charge to the ground:

$$Q = \int_0^{\infty} I(t)dt = \sum_k \frac{I_k}{\omega_k} = 0.047 - 0.767 - 2.5 - 3.06 = -6.3\ C$$

The main portion of the charge is transported by its weak long-term current components. The charge lowered by the basic model is small in comparison with the values of 50 - 100 *C* attributed to standard strokes now a days[29]. Higher values are readily achieved when we increase the model currents by a factor of ten. We will have this factor in mind though. Characteristics of the stroke current will be left invariant, so hereinafter the charge transfer remains constant.

It is not so important for the present study what a particular temporal model is chosen as the basic one, because we are going to modify only geometrical parameters of the stroke. Presence of travelling current wave in the channel is one of the most important details. The wave moves with finite exponentially decaying velocity along the stroke: $V(t)=V_0\exp\{-\omega_V t\}$. The maximum velocity $V_0 = 8\times10^7 ms^{-1}$ is reached at the ground level, and its temporal decay is described by the factor $\omega_V = 2\times10^4 s^{-1}$. Total length of the basic lightning channel equals:

$L = \int_0^{\infty} V_0 \exp\{-\omega_V t\}dt = \frac{V_0}{\omega_V} = 4\ km$. Introduction of the moving current wave is analytically equivalent to the transmission line model[30,33-35]. We will see that the finite velocity $V(t)$ plays a key role in further treatment.

Fig. 2 depicts successive positions of the current wave along the basic return stroke. The amplitude in *kA* is shown along the ordinate. The height or vertical length of the channel is plotted along the abscissa in kilometers. We show spatial distributions of the current along the channel for times t = 49, 69, 99, 122, and 163 μs from the stroke initiation. Correspondingly, the length of the stroke $H(t)$ reaches 2.5, 3, 3.45, 3.65, and 3.85 *km*, respectively. One may see from Fig. 2 that the head of the current wave becomes "compressed" when travelling along the channel. The effect appears due to gradual decay in velocity $V(t)$. Meanwhile, the current waveform $I(t)$ as a function of time remains the same for an arbitrary point Z in the channel[36].

One obtains the spatial distribution of the current along the stroke channel for an arbitrary $t > 0$:

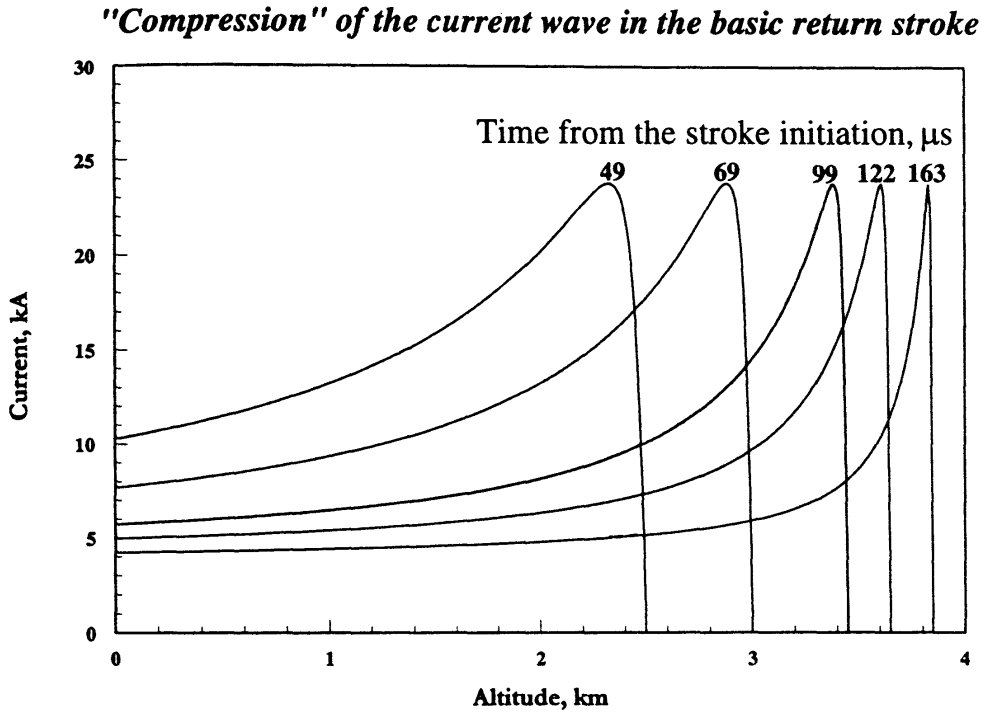

Fig. 2 Progress of the current wave along the channel in the basic model of the return stroke

$$I(t,Z) = \sum_k I_k \exp\{-\omega_k T\} \quad \ldots (2)$$

where $T = \frac{1}{\omega_V} \ln \frac{L-Z}{L-H(t)} \geq 0$, Z is the current coordinate along the channel of the stroke, and $H(t)$ is the height achieved by the tip of the current waves, $0 \leq Z \leq H(t)$[37].

The current moment $M_c(t)$ of the discharge for an arbitrary time t is an integral of the current distribution eq. (2) along the height Z[30]:

$$M_C(t) = \int_0^{H(t)} I(Z,t)dZ =$$
$$V_0 \sum_{k=1}^{4} \frac{I_k}{\omega_V - \omega_k} \left\{\exp(-\omega_k t) - \exp(-\omega_V t)\right\} \quad t>0 \quad \ldots (3)$$

The charge and radiation moments of the stroke are the integral and the time derivative of the current moment are given at eq. (3). It is easy to obtain the following relations:

$$M_Q(t) = V_0 \sum_{k=1}^{4} \frac{I_k}{\omega_v - \omega_k} \left\{ \frac{\exp(-\omega_v t)}{\omega_v} - \frac{\exp(-\omega_k t)}{\omega_k} \right\} \ldots (4)$$

and

$$M_R(t) = V_0 \sum_{k=1}^{4} \frac{I_k}{\omega_V - \omega_k} \left\{\omega_V \exp(-\omega_V t) - \omega_k \exp(-\omega_k t)\right\} \quad \ldots (5)$$

Eq. (4) accounts for the maximum of the static field just before the stroke onset $t \leq 0$; correspondingly, the quasi-static charge moment at this time is of the greatest negative value $M_Q = -V_0 \sum_{k=1}^{4} \frac{I_k}{\omega_V \omega_k}$ $t \leq 0$.

After the stroke initiation, the positive charge flows from the ground to the cloud. Amplitude of charge moment progressively decreases from initial negative value to zero level during a few milliseconds[36].

The positive vertical strokes transport electrons upward, and hence their initial charge moments are positive. We will see that quasi-static field from the stroke plays the role of a 'podium' supporting the transient electric fields in neutral atmosphere.

Frequency dependence of the current moment is found on applying the Fourier transform to the eq. (3):

$$M_C(\omega) = V_0 \sum_{k=1}^{4} \frac{I_k}{\omega_V - \omega_k} \left\{ \frac{1}{\omega_k - i\omega} - \frac{1}{\omega_V - i\omega} \right\} \quad \ldots (6)$$

Spectra of charge and radiation moments are obtained by dividing and multiplying eq. (6) by $i\omega = i\,2\pi f$. The amplitude spectrum $|M_C(f)|$ in the ELF frequency range is given in Fig. 4.

3.2 *Extended Vertical Stroke*

We modify the inverse time constant ω_V of the current velocity to expand the length of the stroke. We use a series of ω_V values that are linked to a set of stroke length, relevant parameters are listed in Table II. Here the stroke length of 4 km corresponds to the basic return stroke model.

We show the computed $M_C(t)$ dependence for the basic and extended strokes in Fig. 3. Time in microseconds is plotted along the horizontal axis on logarithmic scale. The current moment $M_C(t)$ in $kA \times km$ is shown on linear scale along the vertical axis. The lowest curve represents evolution of the current moment for the basic model with vertical channel 4 km long. The peak value $M_C(t) = 3.8 \times 10^7\ A \times m$ is reached at the time $t \cong 50\ \mu s$ from the discharge onset. We show corresponding length of the channel L in the plot. One may see that vertical extension of the stroke makes the peak values greater, and each of them is situated over progressively larger time delay. Parameters of maxima in $M_C(t)$ are listed in Table II as well.

Fig. 4 also depicts the amplitude spectra of current moment $|M_C(f)|$ for the extended vertical strokes.

Table II

Maxima of the current moments $|M_c(f)|$ for the vertical return strokes

Stroke length L km	Speed decay factor $\omega_v s^{-1}$	Maximum of $\lvert M_c(f)\rvert kA \times km \times s$	Time of maximum μs
4	2×10^4	38	50
9	8.9×10^3	56	90
20	4×10^3	79	190
40	2×10^3	110	390
80	1×10^3	147	630

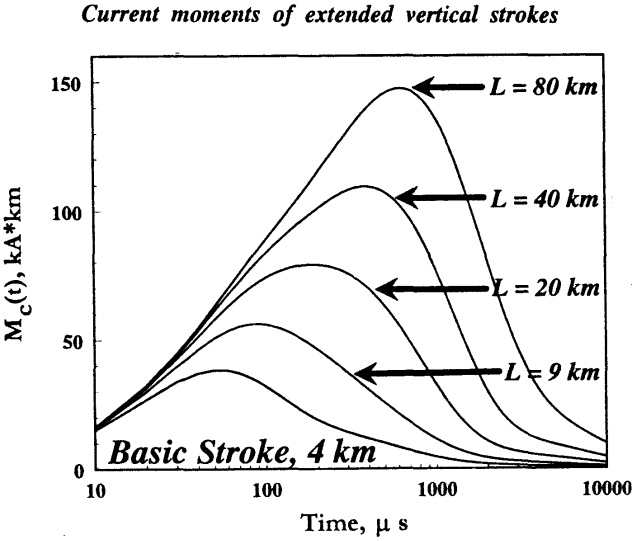

Fig. 3 Temporal variations of the current moments $M_C(t)$ for basic and extended vertical strokes. Maxima grow and retard from 50 to 630 μs with an extension of the channel L from 4 to 80 km.

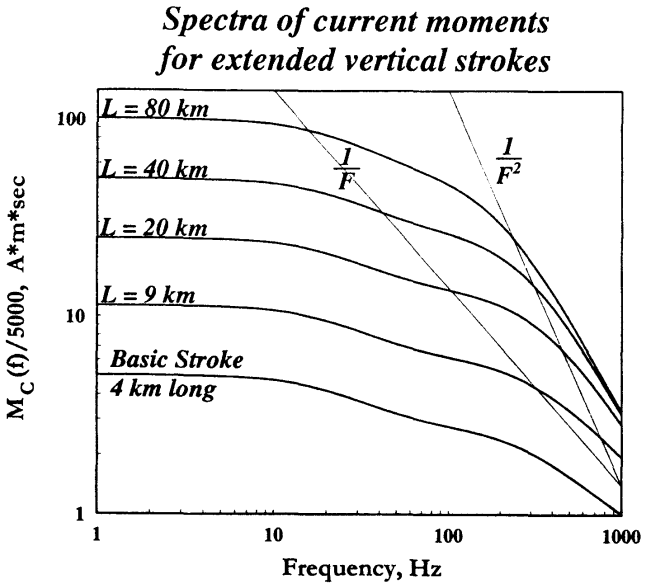

Fig. 4 Amplitude spectra of the current moments $|M_C(F)|$ for basic and extended strokes. Spectra increase with the length of the channel L, and cocentrate over the lower ELF frequencies. Assisting lines show the $1/F$ and $1/F^2$ dependence. The source radiation is flat over the frequency interval where $M_C(F)$ is parallel to $1/F$, and it starts to fade at higher frequencies.

Note again that the lowest curve corresponds to the basic model. One may see the shift of the current moment to the lower ELF when the length of vertical stroke grows. We also plot $1/F$ and $1/F^2$ dependencies in Fig. 4. The frequency region where $|M_c(f)|$ decays

Dr. M-Hayakawa-PM/Mac

as $^1/_F$ corresponds to the flat frequency dependence of radiation moment. The decays at higher frequencies indicate the roll-off in electromagnetic radiation of the stroke.

The vertical return stroke 80 *km* high generates the current moment that reaches its maximum value at approximately 1 *ms* having the decay time of about 3 *ms* (Fig. 3). The spectrum of the current moment for such a stroke is shifted to the lower ELF - ULF band. Electromagnetic energy radiated by vertical return stroke starts decaying at frequencies greater than 100 Hz. Hence, the long vertical return stroke could be an excellent source for the *Q*-bursts. Unfortunately, observations of such strokes were not reported in the literature.

Vertical 80 *km* channel reaches highly conducting layers of the ionosphere and may become a short-circuit between the 'electrodes' of spherical capacitor formed by the Earth and the ionosphere. The capacitor carries a voltage of some hundred kilovolts. Therefore it would be quite natural when such a short-circuit serves as a source of EM signal due to current that grounds positive potential of the ionosphere.

Let us estimate basic properties of such a source. A conducting link abruptly appears between the charged Earth and the ionosphere. The positive current flows to the ground, and it is terminated after the voltage in the system is reduced to zero. Capacitance of the spherical Earth-ionosphere cavity equals $C = \frac{4\pi\,\varepsilon\,a^2}{h} = 10^{-5}\ F$, where ε is the dielectric constant of free space $F\times m$, $a = 6.4\times10^6\ m$ is the Earth's radius and $h = 60\ km$ is the effective height of the ionosphere. The fair weather field of 120 *V/m* exists due to Earth-ionosphere voltage of some hundreds of kilovolts. We accept the value $U = 10^6\ V$. Then, the capacitor carries the charge $Q = 10^{-5}\times10^6 = 10\ C$. The charge transfer by the short-circuit is close to that grounded by a moderate lightning stroke. The current wave of constant velocity $V_0 = 8\times10^7\ ms^{-1}$ will cover the 80 km distance by 1 *ms*. So, we may suppose that the Earth-ionosphere capacitor is discharged in a few milliseconds, which is close to estimates for the extended vertical return strokes. The recovery of ionospheric potential occurs due to current between the Earth and the ionosphere of $j = 2\times10^{-12}\ Am^{-1}$ density. Total planetary current equals 500 *A*. It will rebuild the ionospheric charge and potential in a time from a few to tens of milliseconds.

Summarizing, short-circuit model provides parameters of parent discharge similar to the model of an extended vertical positive stroke of lightning:

(i) They have the same polarity.

(ii) The Earth-ionosphere short-circuit transfers about 10 *C* into 80 *km* distance, having the charge moment of 800 *C-km* (the value is even lower than typical values used for the sprite and *Q*-burst observations).

(iii) Recovery time of the ionospheric potential is in accord with the global rate of *Q*-bursts and sprites.

Hence, we may suggest the following scenario: an energetic cloud-to-ground (CG) positive stroke generates the sprite that is a real conducting channel serving as a short-circuit between the Earth-ionosphere capacitor. This plasma channel exists during some additional time, and it grounds the ionospheric potential producing an intense ELF pulse detected worldwide as a *Q*-burst. Unfortunately, we have no evidence for such sources linked to the ionosphere. Therefore, we proceed with more realistic sources of natural electromagnetic radiation.

3.3 Bent Stroke Model

An extension of the stroke length bestows its current moment in time and increases its lower ELF radiation by the factor directly proportional to the channel length. The energy radiated shifts to 10–100 *Hz* frequency band, and radiation at the higher frequencies decreases. A vertical positive stroke 80 *km* long becomes an excellent candidate for the causative stroke of *Q*-bursts and slow tails, producing the fields 20 time higher than an ordinary stroke 4 *km* high. Still, such long vertical channels have never been observed.

A rather straightforward idea appears of preserving the channel length, i.e., the stroke bending. Consider a lightning discharge formed by vertical and horizontal branches. Its current wave moves initially upward to altitude Z_p and then it turns horizontally. Vertical and horizontal branches will produce intense repetitious pulses in the vicinity of the stroke facilitating the modifications of the atmosphere[36]. We will discuss this feature below.

Horizontal part of the channel is an ineffective source for ELF fields, since these waves propagate in the TEM mode within the Earth-ionosphere cavity[38,39]. Nevertheless, we may hope that vertical component of the current moment of the bent discharge becomes longer in comparison with vertical return stroke Z_P *km* high, because there exists a vertical 'tail' of the current wave that had already turned in horizontal direction. Unfortunately, this is not so[37]. Fig. 5 demonstrates that the current moment of the bent stroke rapidly decays after the 'head' of the current wave passes the turning height Z_P and the horizontal motion begins. The figure includes two frames. The upper one depicts the current moments $M_C(t)$ in the time domain. The lowest curve here depicts the basic model 4 *km* long. Other curves show variations pertinent to the strokes of various lengths (9, 20, and 40 *km*) and having the same turning altitude $Z_P = 4\,km$. The lower frame demonstrates small modifications present in the spectra on the current moments.

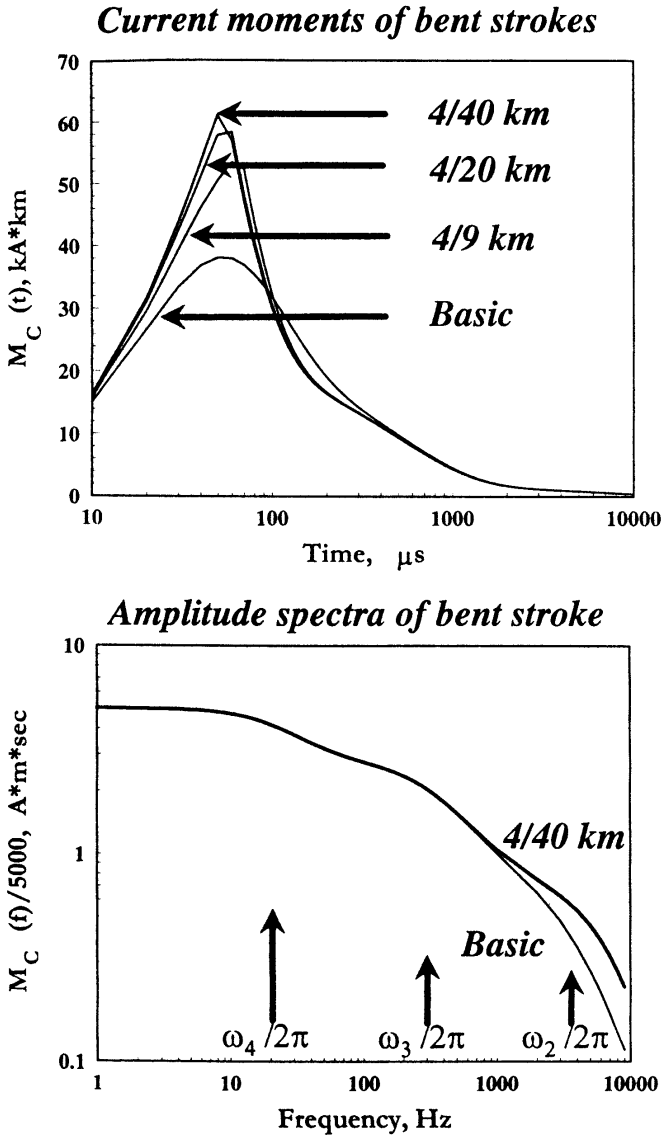

Fig. 5 The current moments of bent strokes with part 4 km long. Duration of $M_C(t)$ remains practically unchanged, while its onset becomes steeper for longer strokes. Therefore, longer strokes have slightly enhanced VLF component (lower frame). Vertical arrows indicate characteristic frequencies of the second, third and fourth terms of the stroke current in eq. (1), where small humps are seen.

These discouraging results are explained as follows. In the model of basic stroke, the current rapidly decays at the base. Its maximum shifts to upper parts of the channel, which determine the current value of $M_C(t)$. As a result, the current moment varies not so fast as the current itself. Situation is different for a bent stroke. Vertical branch rapidly looses the current after the wave starts horizontal motion. No widening occurs in the vertical component of $M_C(t)$ despite the current wave proceeds horizontally. Hence, the bending of the stroke does not intensify its ELF radiation component regardless the complete travelling time of the current wave grew. Moreover, the front of the pulse becomes steeper when the stroke length increases. Correspondingly, the VLF component of the amplitude spectrum becomes slightly elevated for the bent stroke, see Fig. 5 lower frame. Hence, the bent stroke fails to enhance the ELF component in the current moment.

3.4 "Staircase" Stroke Model

The 'staircase' or multiple bent stroke is a further and effective modification of stroke geometry. Such a stroke consists of vertical and horizontal branches (see Fig. 6). The first vertical branch starts from ground and ends at Z_{P1} altitude (turning point of the current wave). From here, the current wave moves in a horizontal direction along the path L_{P1}. After the wave reaches the second turning point, it proceeds along the vertical direction again, etc.

The lower part in Fig. 6 demonstrates the current allocation in the channel at the final stage of the stroke. As demonstrated in Fig. 6, the vertical parts (1), (3), (5) serve as the sources of transverse magnetic TM wave. Connecting horizontal channels (2), (4), (6) shown as shaded stripes do not contribute to the distant ELF fields. These horizontal sections of the

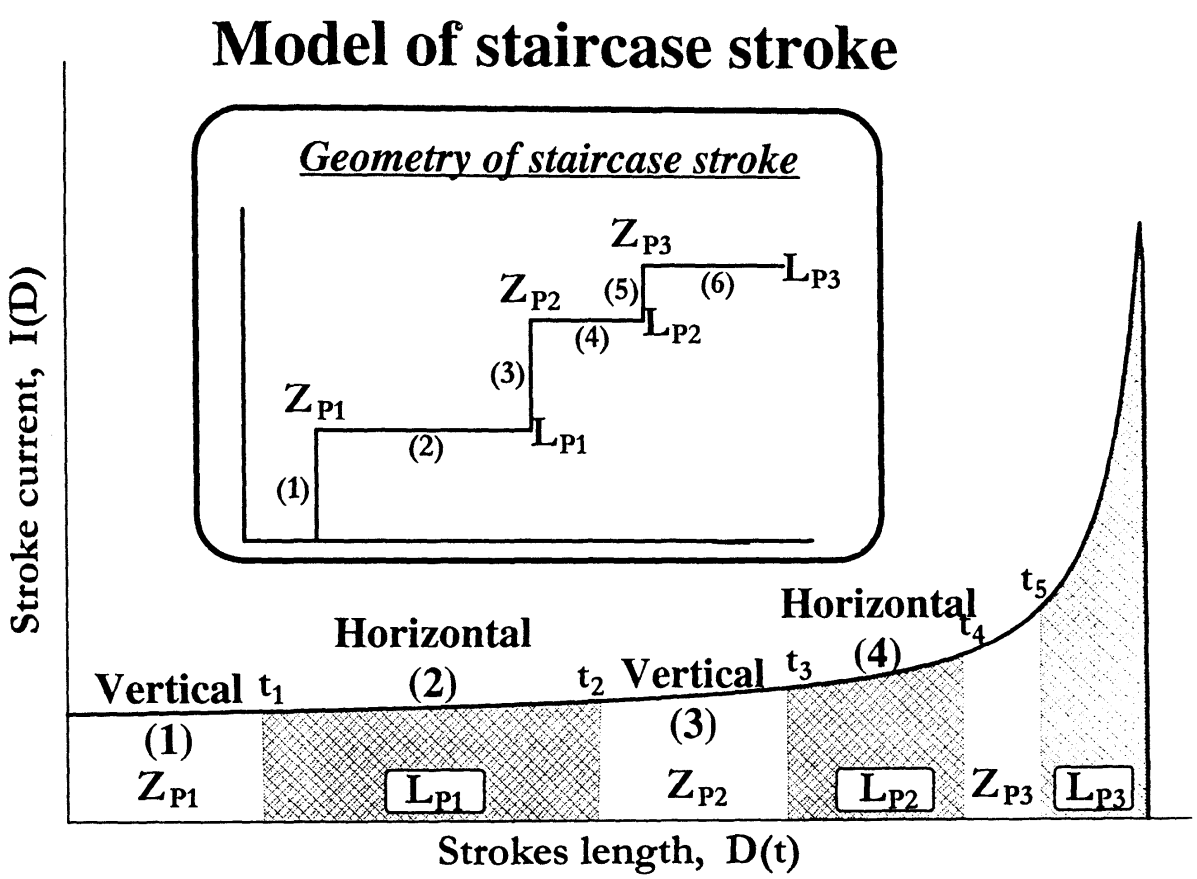

Fig. 6 Geometry of an arbitrary channel and its partition scheme. The final stage of movement of the current wave is depicted. The shaded zones represent horizontal parts of the stroke channel. Turning times of the current wave t_p are indicated.

channel need not be collinear as we show in the figure. Their orientations may substantially deviate, which allows the long stroke to be a relatively compact structure.

Vertical sections are important sources for travelling waves. Each branch of the staircase stroke is a source of EM field near the source. Since the current wave arrives to individual sections with a delay, the pulses are retarded forming a series in time and space. Their arrival times, amplitudes and alignments of the electric field depend on the orientation of individual sections with respect to an observer placed in the atmosphere above the ground. Multiple pulses may produce electron acceleration and focusing in the disturbed atmosphere above a thunderstorm. We discuss these features below. Here we pay our attention to vertical component of M_C in a staircase stroke.

When a current wave moves along the channel, its turning times are $t_1 = \frac{1}{\omega_v} \ln \frac{V_0}{V_0 - Z_{P1}\omega_v}$, (the first turn toward the horizontal motion), $t_2 = \frac{1}{\omega_v} \ln \frac{V_0}{V_0 - (Z_{P1} + L_{P1})\omega_v}$ (the recovery of vertical propagation), etc.

For an arbitrary number of branches or turning points, the vertical component of the current moment in time domain is found from[37]:

$$M_C^K(t) = \int_0^{H(t)} I(l,t)dl = S_1(t) - \vartheta(t)S_2(t)$$

$$+\sum_{n=1}^{K-1}(-1)^n \sigma(t-t_n)S_1(t-t_n)\exp(-\omega_v t_n) \qquad \ldots (7)$$

Here the integer number K denotes the number of turns in the channel. This number is odd $K = 2m+1$ when the channel ends by a horizontal branch. It is even $K = 2m$ when the stroke ends by a vertical section. t_n is the time of n-th turn of the current wave,

$$S_1(t) = \sum_k \frac{V_0 I_k}{\omega_v - \omega_k}\exp(-\omega_k t) \qquad \ldots (8)$$

$$S_2(t) = \exp(-\omega_V t)\sum_k \frac{V_0 I_k}{\omega_V - \omega_k} \quad \ldots (9)$$

$$\vartheta(t) = \begin{cases} 1, & t \in (t_{2M}; t_{2M+1}] \\ 0, & t \notin (t_{2M}; t_{2M+1}] \end{cases} \quad \ldots (10)$$

$$\sigma(x) = \begin{cases} 1, & x > 0 \\ 0, & x \le 0 \end{cases} \quad \ldots (11)$$

The current moment in the frequency domain is found by the Fourier transform over the intervals $(0, t_1)$, (t_1, t_2), ..., (t_{K-1}, ∞):

$$M_C^K(\omega) = \int_0^\infty M_C^K(t)\exp(-i\omega t)$$

$$= M_C(\omega)\left\{1 + \sum_{n=1}^{N}(-1)^n \exp\left[-(i\omega + \omega_V)t_n\right]\right\} \quad \ldots (12)$$

where $M_C(\omega)$ is the spectrum of the vertical return stroke eq. (6) having the same complete length of the channel L as the staircase discharge has.

We illustrate the results for the staircase stroke with two vertical and single horizontal branches in Fig. 7. This is the simplest possible model, still it pertains to all the features of the staircase stroke. The upper frame in Fig. 7 demonstrates temporal variations. Initial part of plots is similar to those shown in Fig. 6. Time in μs is plotted along the abscissa on logarithmic scale, and the current moment in *kA* x *km* is shown along linear vertical scale. We repeat the $M_C(t)$ function for the bent stroke 40 *km* long having the 4 *km* vertical part and that for vertical lightning discharge of 20 *km* (dashed line). Also, we plot three new curves pertinent to different staircase strokes. The channel length is L=20, 30 and 40 *km*. All the models of staircase stroke have the same partition ratio: the initial vertical branch equals $Z_{p_1} = 0.7\ L$, its horizontal part is $L_{p_1} = 0.7\ L$ long, and limiting vertical portion is $Z_{p_2} = 0.2\ L$. It is clear that the bent and staircase strokes 40 *km* long have similar structure, with the only difference being in the vertical 8 *km* ending part of the staircase model. Therefore, we may expect that the current moments of both the models will have much in common.

Since the model stroke has two vertical elements, the vertical component of its current moment contains two pulses. This fact is illustrated in Fig. 7. The secondary delayed pulse appears when the current wave starts travelling along terminating vertical branch of the channel. Mutual time delay grows with the length of horizontal branch or with the complete length of the model stroke. As we had expected, initial parts of plots completely coincide for staircase and bent channels with $L = 40\ km$.

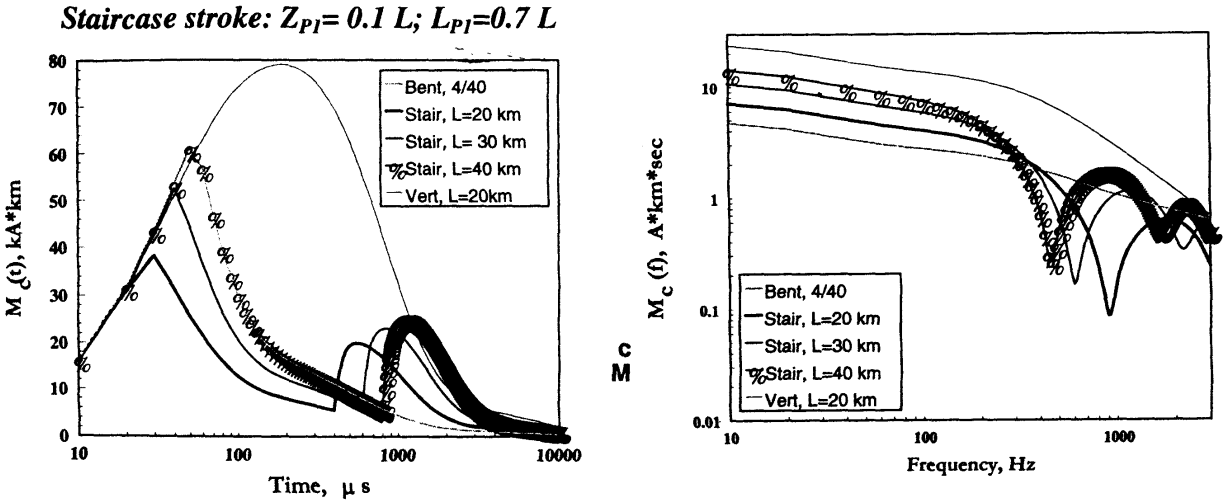

Fig. 7 Current moments of the staircase stroke in time and frequency domains. A three element staircase stroke provides a pair of pulses. Their similarity and deviations from the bent 4/40 km stroke are vividly seen. Pulses interfere in the spectral domain, as is shown in the lower frame.

Simultaneously, the decay of secondary pulses in the staircase strokes is close to that of vertical $L = 20\ km$ discharge. Temporal decay of current wave velocity makes the secondary pulses lower and wider in comparison with initial ones.

Secondary pulse of the current moment modifies amplitude spectra shown in the lower frame of Fig. 7. Here, the abscissa shows the frequency, and the ordinate depicts the current moment *MC(f)* in *AxkmxSec* on logarithmic scales. General behaviour of the spectra is similar to that of an extended vertical stroke. The secondary pulses cause an interference pattern. Position of spectral nodes depends on the pulse delay. One may see that the line showing the spectrum of 40 *km* staircase stroke fluctuates around the curve representing the bent 4/40 km discharge.

Spectra in Fig. 7 illustrate concentration of the current moments over the lower ELF. This shift is explained by widening of the ELF pulses from staircase stroke. Horizontal portion of staircase stroke does not contribute to vertical component of the current moment. Therefore the amplitude of electromagnetic radiation from a staircase stroke is always reduced in comparison with the vertical discharge of the same length. Its amplitude at lower ELF, coincides with that one of an extended vertical stroke of the length that is equal to the complete extent of vertical sections in the staircase stroke[37]. Waveforms of the current moment shown in Fig. 7 resemble the plots published by Stanford University group[40]. Our goal was an enhancement of ELF radiation by geometrical modifications of the lightning model. Similar goal was pursued by Pasko *et al.*[40], who intended to show that the slow-tails may originate simultaneously with the red sprites. They met a problem of insufficient stroke duration when modelling both the non-linear effects in the ionosphere and associated slow-tail atmospherics. An exotic solution had been found by introducing a current induced in the conducting body of the sprite. This current radiates the secondary ELF pulse[40].

Our model is much simpler and looks more natural. All we had done with a standard model of the return stroke was an extension in length and bending. We demonstrate below that bent strokes produce multiple electric pulses in the atmosphere. This makes them a solid candidate for the sprite producing lightning[36].

Fig. 8 separately shows $M_C(t)$ and $|M_C(F)|$ for the staircase stroke 80 km long. Its horizontal size is close to the biggest reported in the literature. Partition scheme was the following: initial vertical part of the channel equals 4 *km*, while its terminating vertical section is 8 *km* high. The rest 68 *km* of the channel are horizontal (compare the channel length with Krehbiel *et al.*[56]). Upper frame in Fig. 8 demonstrates the $M_C(t)$ dependence. Time in milliseconds is plotted along the abscissa on linear scale, and the current moment in *kAxkm* is shown along vertical axis. Turning times of the current wave are $t_1 = 51\mu s$ and $t_2 = 2.3\ ms$. The pulses are completely different. The first one is rather sharp, and the secondary pulse is much wider. It looks so wide and so slow that the pulse itself could be taken for a huge continuing current of the stroke (see also the Fig. 9).

Two lower frames in Fig. 8 depict the spectra on bi-logarithmic scale. Intermediate frame compares spectrum of the staircase stroke with that of equivalent vertical discharge 12 km high. Interference between initial and secondary pulses concentrates radiation in the lower part of the ELF range. It provides also a series of spectral minima, the first of them occupies the 150 *Hz* frequency. The interference also forms the 'roll-off' of the spectrum.

Fig. 8 shows how an ordinary stroke becomes a powerful source of the ELF radiation due to geometrical extension of its channel. The current and charge transfer remained invariant in the model. Geometrical modifications allowed to avoid the problem of enormous charge transfer pertinent to other models of the sources of ELF transients.

Experimental studies of ELF transient events (Q-bursts) showed that spectra of their sources contain an elevated ELF part[8,20]. Observations of distant slow-tail atmospherics in the Earth-ionosphere waveguide also indicated that spectra of the causative discharges had a distinct maximum over some hundred *Hz* frequency[22,41,42]. It had been concluded that the Q-burst and slow tail signals were caused by lightning strokes with outstanding continuing currents. We list experimentally estimated time constants in Table III. First column in this table shows the references. The second one demonstrates frequency band of measurements, and the last two columns show average decay constants of the current moment of the source strokes.

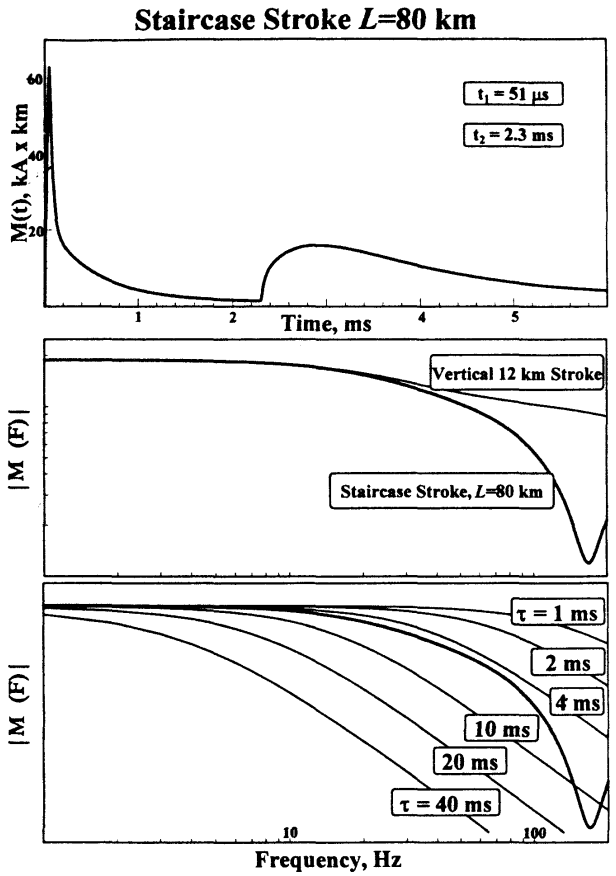

Fig. 8 Current moment of the staircase stroke 80 km long. The upper frame shows the temporal variations. Note that secondary pulse may be confused with huge continuing current. Middle frame illustrates an impact of pulse interference on the spectrum. Lower frame compares the staircase spectrum with the those of exponentially decaying current moments, relevant decay constants are shown in the figure.

Table III
Time constants of parent strokes deduced from ELF measurements

Investigator	Bandwidth, *Hz*	Time constant, *ms*	
		Positive stroke	Negative stroke
Burke and Jones 1996	5 - 50	32	26
Huang et al. 1999	4 - 120	5.4 (sprites), 3.6 (elves)	
Marshall et al. 1998	5 - 5,000	1-2	

In principle, the staircase stroke model allows obtaining any frequency decay by varying the partition of the channel. We compare the model spectrum with experimental data in the lowest frame of Fig. 8. Here we show the staircase spectrum and those computed for different exponential time decays in the current moment, $\tau \in [1, 40]ms$. Frequency dependence for our staircase stroke corresponds to measurements by MIT group[8].

Now, we consider a complicated, more realistic and convincing model: the multiple bent staircase stroke having many turns in the channel (Fig. 9). We choose the equidistant partition scheme, when a stroke consists of elements having the standard sizes (see the inserted panel in the upper frame of Fig. 9). The channel starts vertically and reaches 4 *km* altitude. Then, it turns in a horizontal direction and has the length of 17 *km*. The following vertical and horizontal elements are correspondingly 2 and 17 *km* long, respectively . The numbers over vertical bars in Fig. 9 indicate the ending altitudes. The numbers below horizontal segments indicate their length. As in the model shown in Fig. 8, the stroke reaches 12 *km* altitude, and its total horizontal length equals 68 *km* (the form and orientation of horizontal elements may be arbitrary, compare with Krehbiel *et al.*[56].

We plot the current moment $M_C(t)$ in the upper panel of Fig. 9. Time delay is shown on the abscissa in *ms*. Since the stroke has five vertical elements, the vertical component of its current moment contains five pulses. Their width and onset times progressively increase because the velocity of the current wave exponentially decays in time. The last, fifth pulse is so wide and small that it may be confused with the stroke continuing current.

The succession of pulses in $M_C(t)$ causes the spectral modifications shown in lower frame of Fig. 9. Frequency in *Hz* is depicted along abscissa. The spectra $M_C(F)$ are shown on ordinate in *kAxkmxs*. The logarithmic scales are used on both axes. Spectrum of the vertical stroke 12 *km* high is also shown in figure as reference. One may see that the staircase structure provides an increase of spectral components over Schumann resonance band and around 300 Hz frequency.

There exists a temptation to explain the experimentally testified increase over the lower ELF by a great amplitude and an enhanced continuing current in the causative strokes. Still, one meets considerable difficulties when applying such a

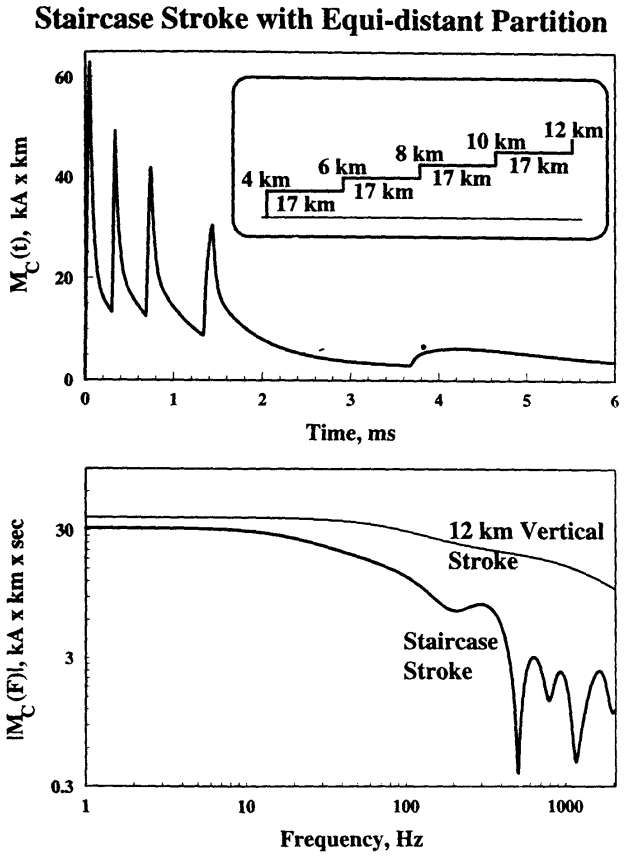

Fig. 9 Waveform and spectrum of the current moment for the staircase stroke model with equidistant partition. The structure of the channel and the relevant $M_C(t)$ dependence are shown in the upper frame. Each horizontal section is 17 km long vertical parts end at altitudes of 4 6, 8 10 and 12 km. The lower frame shows the spectra of equivalent lightning flash 12 km high and that of the staircase stroke enhanced over the Schumann resonance band and around 300 Hz frequency.

'straightforward' solution: extremely large lengths of the channel and great charge transfers must be implemented[8,41,42]. A model of the staircase channel is able to simply shift the whole radiation into the 100 Hz range, while the stroke power characteristics remain invariant: the current in the channel and the charge transfer remain the same as in the basic model of lightning. This is the main advantage of the staircase model.

Computations show that a model with equi-delayed pulses provides a regular system of periodical maxima with 2-3 fold increase of the SR amplitude in comparison with equivalent vertical discharge[43].

The following modelling features demonstrate that the form of the channel may substantially alter its current moment:

i) Sole modification of geometrical structure of the stroke may completely alter the waveform of its current moment.

ii) ELF radiation of an expanded bent stroke is associated exclusively with its vertical branch, and no enhancement occurs with its horizontal section.

iii) Staircase stroke generates multiple pulses that become progressively wider and smaller in amplitude. Strongly delayed terminating pulse may be confused with the stroke continuing current.

iv) Depending on the partition, the staircase stroke may enhance the ELF fields up to an order in magnitude, while its current and charge transfer remain unchanged.

v) Models of extended vertical and staircase lightning strokes fit the results of observations of the slow tails and of Q-bursts in the Schumann resonance range.

4 Nearby Fields from Model Strokes in Neutral Atmosphere

We demonstrate here the nearby electric fields of a bent discharge in the time-space domain. Computations included the static, induction and radiation fields. Reflections from the perfectly conducting ground were included into solution by introducing the image sources. The reflections from the ionosphere were ignored. Atmosphere was assumed to be neutral[36]. Such an assumption is justified when the displacement currents are much greater than currents of conductivity in the air. We plot the cutoff frequency of nocturnal atmosphere as a function of altitude in Fig. 10. The dependence was adapted from Hale[44] and Hale[45] on middle-latitude night conductivity profile, since the optical events were observed at these latitudes during the night. The cutoff frequency at a given altitude was found from the following condition: $\sigma(h) = \varepsilon\, \omega_{CUT-OFF}(h)$. Atmospheric conductivity in tropics is approximately an order of magnitude lower than Fig. 10 shows. Hence, the same profile is valid there shifted to the left by a single strip[44,45]. Fig. 10 indicates that rapidly varying fields penetrate to higher altitudes. Say, a sinusoidal signal of 1 *Hz* frequency will be reflected from the altitude around 45 *km*, while the signals of Schumann resonance may penetrate to approximately 70-80 *km*.

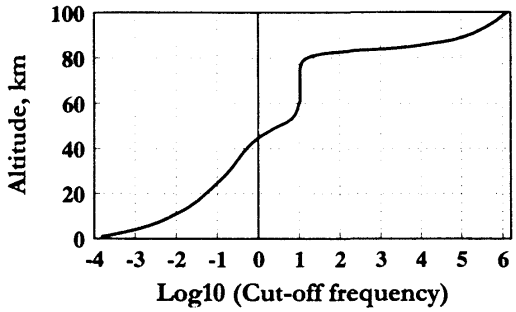

Fig. 10 Profile of cut-off frequency governed by night coductivity of middle-latitude atmosphere $\omega_{CUT\text{-}OFF} = \sigma/\varepsilon$ (adapted from Hale[44]).

One may use this diagram to estimate an altitude where the electric fields may reach from a lightning discharge at night. Since the characteristic time for the current moments is a few milliseconds long, the characteristic frequency is around some hundreds Hertz, and the night atmosphere may be regarded as a neutral medium up to 70-80 *km*. We show the diagrams computed at 50 *km* altitude.

We will model the signals in neutral atmosphere produced by strokes with more complicated geometry than simple vertical channel has. Only the simplest cylindrically symmetric models were used in attempts to model processes in the middle atmosphere caused by lightning[5,6,11,42,46-49]. The reason is that a linear electrodynamic problem is not easily resolved in an atmosphere with a conductivity profile when the source has an arbitrary geometry. The progress had been achieved with axially symmetric quasi-electrostatic fields, Maxwell currents and an impact of local tropospheric disturbance on their distribution[34,50-53].

Meanwhile, experimental results indicate that horizontal sections of the source currents must be included into consideration. For instance, Marshall *et al.*[22] measured the low frequency electromagnetic pulses from the strokes that caused elves. The signals contained a tweek atmospheric component. This directly verifies an existence of a horizontal current in the stroke, otherwise, the tweek signals would not appear[26,54].

When computing near-zone fields, we used the following models: extended vertical return stroke, positive stroke initiated either from the ground or from the cloud, bent discharge, and 'spider' stroke[36]. Combination of channel bending and delays of the current wave of individual sections results in multiple pulses emerging in the atmosphere. Our modelling had shown that many pulses vanish at the perfectly conducting ground which substantially limits the suitability of the ground-based electromagnetic observations.

Electric field in a neutral atmosphere acquires transient components: vertical, inward-outward and sideways, and therefore it 'scans' the sky. Fields from energetic lightning strokes are of the level enabling them to initiate the plasma process in the rarefied air. Still, we will not consider a self-consistent problem of non-linear interaction between radio wave and the medium. The geometry of a bent stroke model we use is shown in Fig. 11. The current wave starts from the ground vertically and turns in a horizontal direction at altitude $z_1 = 5$ *km*. When computing the fields shown in Fig. 11, we specify the length of the lightning channel $L = 10$ *km*. Initial velocity of the current column equals $V_0 = 8 \times 10^7$ ms^{-1} and its decay factor $\omega_V = 8 \times 10^3$ s^{-1}. The observer is situated at the 50 *km* altitude and is displaced from the discharge in horizontal direction by a distance D. The horizontal branch of the lightning stroke makes the angle ψ with the direction from the stroke, grounding to the observer being the X-axis of coordinate system.

Three separate frames in Fig. 11 show temporal variations of the electric field at 50 *km* altitude. Lower left frame depicts the transverse horizontal field component $E_y(t, D)$ for D = 10, 25, and 50 *km* and for the perpendicular orientation of the channel (orientation 'across'), i.e., when $\psi = \pi/2$. Static and induction fields are responsible for slow variations of these plots having the scales of milliseconds, while the radiation field creates the fast transient pulses. An abrupt negative pulse appears in $E_y(t, D)$ dependence when the current wave starts moving horizontally. Afterwards, the wave reflected from the ground arrives, and the positive pulse begins with the subsequent slow decay to zero level.

Two right frames demonstrate variations in horizontal parallel $E_x(t, D)$ and vertical $E_z(t, D)$ components for the case $\psi = 0$ (the channel orientation 'along'). Huge and slow quasi-static field is present in the vertical electric field at close distance. Two delayed pulses of opposite sign appear due to direct and reflected from the ground wave.

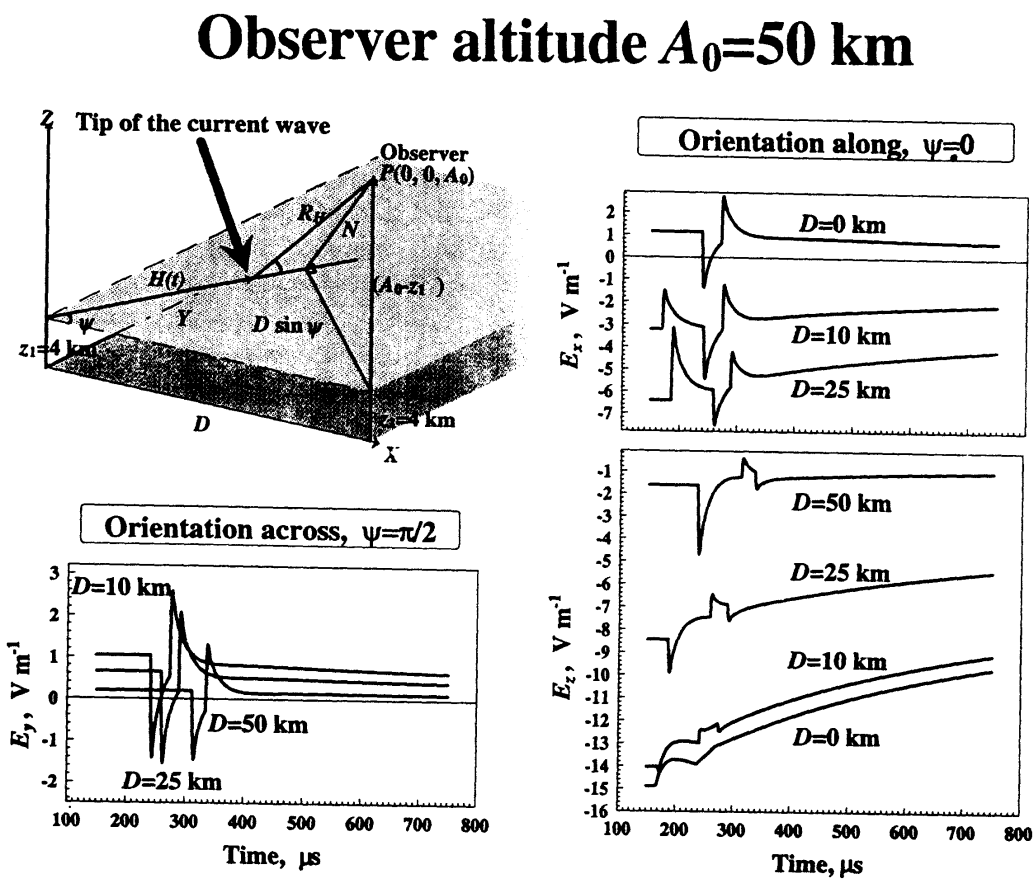

Fig. 11 Geometry of the stroke. Vertical and horizontal electric field components at altitude 50 km over the perfectly conducting ground. Two possible orientations of the channel are modelled $\psi = 0$ and $\psi = \pi/2$.

Frames in Figs. 11 and 12 demonstrate the dynamics of electromagnetic pulse in neutral atmosphere at short distances from the discharge. The main feature of the bent stroke is the multiple pulses of altered signs (directions). Analysis shows that only bent strokes generate such signals. For instance, the spider stroke is regarded in the literature as a promising candidate for atmospheric modifications[8], but it does not produce any noticeable pulses. The umbrella-like structure of upper part of the spider stroke provides mutual compensation of individual pulses arriving from separate horizontal limbs. Only positive stroke with the current wave moving from the cloud to the ground (an extraordinary motion) generates dual pulses[36].

Fig. 12 shows in more details the dynamics of electric field at 50 *km* altitude for the across orientation of the horizontal channel ($\psi = \pi/2$). Computed data for all three field components are presented as the 3-D plots over the delay-distance plane. Such a presentation clearly shows the propagation of the transient fields.

We computed the electric fields in the neutral atmosphere using the stroke models of different geometry. The reflections were included from perfectly conducting ground into computations. The results obtained may be summarized as follows:

i) Positive cloud-to-ground discharge initiated from the top of the lightning channel produces dual pulses.

ii) Bent lightning channel doubles the number of radiated pulses. Combination of vertical and horizontal currents increase the amplitude of the transient electric field. This field depends on the orientation of horizontal sections in the stroke. The static field persists for some *ms* until the vertical charge dipole moment is present.

iii) Branching of the stroke results in the decrease of its radiation from horizontal currents because of the subtraction of individual pulses. The horizontal part of symmetrical spider lightning stroke does not produce substantial electromagnetic radiation at all.

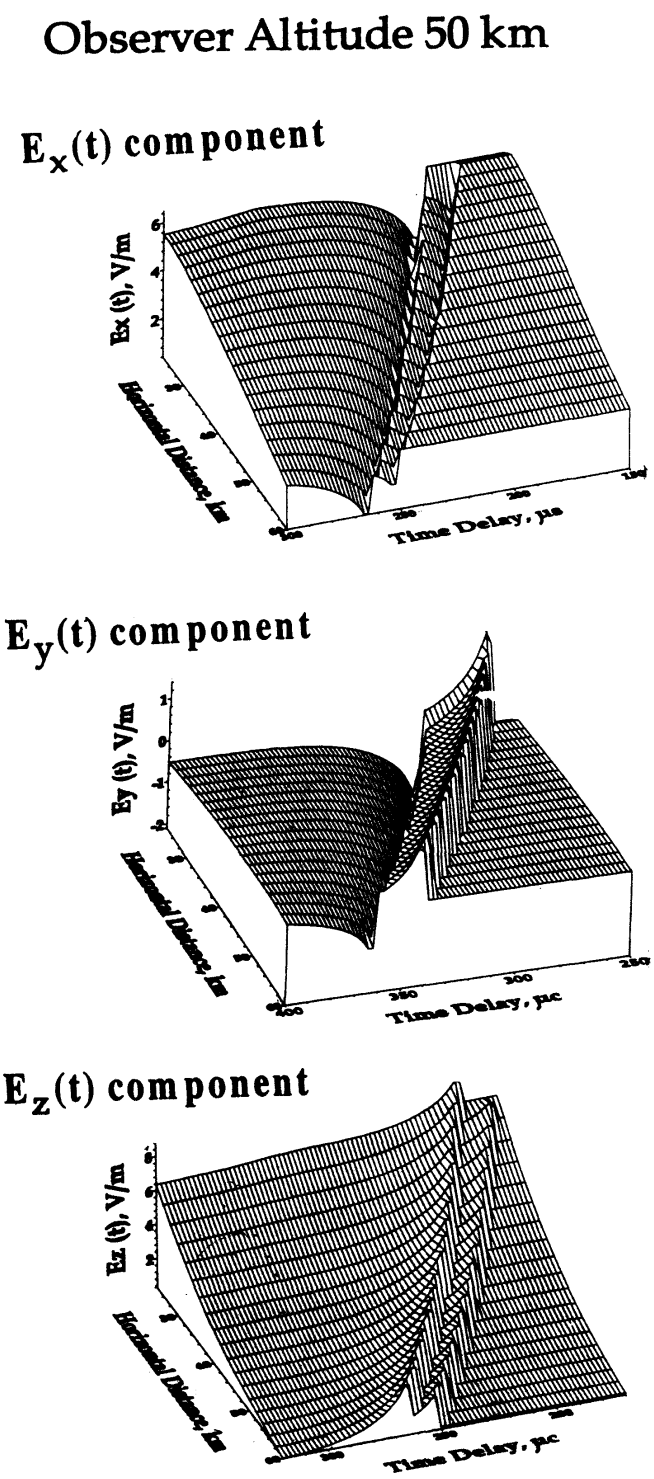

Fig. 12The 3-D plot above the distance-delay plane of the electric fields produced by a perpendicular bent stroke of lightning

iv) Transient fields vanish above the stroke and tend to decrease at the ground surface, Therefore, the high altitude airborne observations should be used to detect the pulses.

v) The electric field may accelerate free electrons in vertical and horizontal (radial and sideways) directions at the onset of the pulse. A focusing of particles may occur at distances between 25 and 75 *km* from the stroke.

vi) Density and temperature disturbances in the atmosphere above a thunderstorm may contribute to the initiation of the plasma process. Both the disturbances and electron focusing are enhanced toward the periphery of a storm, so the luminous structures must be expected at some distance from the parent discharge.

5 ELF Propagation Model

Since staircase strokes are the best possible candidates for the parent discharge for optical emissions and ELF transients, we consider the influence of subionospheric radio wave propagation on the signals originating from such strokes[55]. Modelling will show the evolution of ELF pulses travelling in the Earth-ionosphere waveguide. We demonstrate that a staircase stroke initially launches a succession of pulses into the duct, but the wave dispersion and attenuation quickly transform them into a sole pulse.

At frequencies below 1.5 kHz, the single transverse magnetic (TM) mode propagates having two non-zero field components at the surface of perfectly conducting ground[18,38,39]:

$$E_r = \frac{i\nu(\nu+1)}{\omega}\,\frac{M_C(\omega)}{4a^2h\varepsilon}\,\frac{P_\nu\left[\cos(\pi-\theta)\right]}{\sin\pi\nu} \qquad \ldots (13)$$

$$H_\varphi = -\frac{M_C(\omega)}{4ah}\,\frac{P_\nu^1\left[\cos(\pi-\theta)\right]}{\sin\pi\nu} \qquad \ldots (14)$$

The above solution was constructed in the spherical coordinate system (r,θ,φ) with the origin at the Earth's centre. The source occupies the pole $(r_s = a;\theta_s = 0;\varphi_s = 0)$, and the observer location is at $(r_o = a;\theta_o = 0;\varphi_o = 0)$. Fields are measured in $V\times s\times m^{-1}$ and $A\times s\times m^{-1}$ correspondingly. $M_C(\omega)$ is the complex spectrum of the current moment of the parent stroke; θ is the angular distance between the source and observer in radians, a is the Earth radius in m,h is the effective height of the ionosphere in m,ε is the dielectric constant of the free space in $F\times m^{-1}$, $P_\nu(x)$ and $P_\nu^1(x)$ are the Legendre and associated Legendre functions, respectively. The propagation parameter of ELF radio wave $\nu(\omega)$ is found from the following linear relation:

$$v(f) = v_1 + iv_2 = \frac{f-2}{6} - i\frac{f}{100} \quad \ldots (15)$$

The propagation model is discussed in details in the previous papers[43,55]. Electric and magnetic fields were computed in the frequency domain for a given spectrum of the source current moment $M_C(\omega)$. Then, an FFT algorithm was applied, and we obtained the time domain solution. We use here the frequency band from 4 to 4096 *Hz*. This meant the 'model receiver' has the ideal rectangular frequency characteristic in this range.

Fig. 13 displays the dynamics of the pulses traveling from vertical and staircase strokes as shown in Fig. 8. Fig. 13 contains two partially overlapping contour maps $E(t, D)$ over the delay-distance plane. Maps have the same scale. The delay from the pulse initiation is plotted on the abscissa and the distance from the stroke is shown along the ordinate. The maps are shifted vertically to facilitate the comparison of the waveforms. The scaling bar for the pulse amplitude in *mV/m* is shown at the right. We use relatively small distance interval from 1000 to 10000 *km* to show details of pulse merging. We depict only vertical electric field component because the profile of horizontal magnetic field practically repeats the electric field in the range up to source antipode.

Upper map shows the rapid merging of two pulses into single wave when propagating in the Earth-ionosphere cavity. The distance from the source in thousand of kilometers is shown along the left ordinate. The lower map is shifted downward and presents the reference evolution of a single pulse originating from the equivalent vertical stroke 12 *km* high. Its propagation distance is shown on the right ordinate. One may see that dispersion and absorption of radio wave in the Earth-ionosphere cavity transforms initially dual pulse into a single peak at around 5000–6000 *km* distance (the upper trail in Fig. 13). At about 10000 *km* distance, the profiles for both vertical and the staircase strokes become indistinguishable, apart from a slightly greater delay from the staircase stroke. This occurs because secondary (delayed and wider) pulse becomes dominant. Merging of individual pulses takes place despite we had chosen the discharge model with an extreme gap between initial sub-pulses. Hence, one may expect that in reality the pulses completely merge at distances shorter than the 5000 *km*. As a result, a remote observer is unable to decide what a particular source had caused the pulse: an energetic vertical lightning discharge or a bent staircase stroke. This conclusion is also valid for the multiple return strokes with the high repetition rate of individual pulses. Still, the complete charge transfer of a multiple stroke equals the sum of charges downloaded by individual strikes. Hence, a multiple stroke spends a greater amount of energy than a staircase discharge does. The latter appears to be a much more efficient source of ELF waves, because all its sections operate on the same current and transfer the same charge.

Maps in Fig. 13 demonstrate that:

i) The waveform of dual pulse alters along the propagation distance. It turns into a single peak at a range around 5000-6000 *km*.

ii) Temporal positions practically coincide with the weighted centre of the dual staircase pulse and of the top of a single pulse from the vertical stroke.

iii) The sharp primary pulse decays faster with distance because it contains higher frequency components characterized by a greater attenuation factor. The second, wider pulse dominates from 5000-6000 *km* distance.

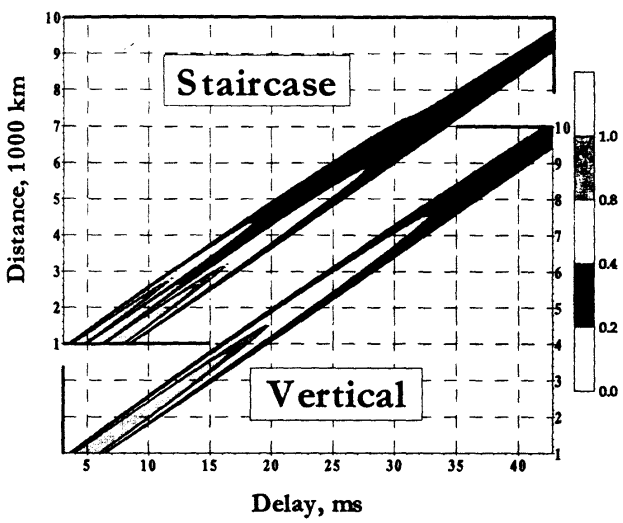

Fig. 13 Space-time evolution of the ELF pulses from the staircase (upper map) and vertical stroke (lower map). Dispersion and absorption of radio wave pertinent to the Earth-ionosphere guiding system transforms initially dual pulse from the staircase stroke into a single one at around 5000-6000 km distance. The pulse profiles become completely similar at 10000 km distance only the pulse from a staircase stroke is slightly delayed with respect to that from vertical stroke.

The model of staircase stroke with two vertical sections connected by single horizontal branch is the simplest one. Real discharges are of more complicated structure. They have various random branches in the current channel. Therefore, the multiple staircase stroke is a more realistic structure. We will show that multiple individual sub-pulses originating from such a stroke coalesce into a single peak when the propagation distance becomes sufficiently great. Dynamics of pulses propagating from the staircase stroke depicted in Fig. 9 are displayed in Fig. 14.

Vertical electric field component $E(t, D)$ had been computed as a function of distance and frequency using eq. (13-15). Fig. 14 includes three frames. The middle one demonstrates the pulse evolution in the Earth–ionosphere duct. Amplitude of the field is shown as a contour map over the delay-distance plane. Delay is shown on the X-axis in milliseconds and the source-observer distance is plotted along ordinate in thousand of kilometers.

We plot a vicinity of the source to resolve initial pulses and demonstrate their quick merging due to influence of the guiding system. Initially, the waveform from the staircase stroke contains the same number of pulses as the causative discharge had. The shortest source-observer distance in Fig.14 is comparable with the horizontal size of the parent stroke. Therefore, we had postulated that all the distances from the observer to individual vertical sections of the stroke are the same. In other words, there was no additional propagation delay and amplitude modification by this distance factor. (We do not consider here a peculiar situation when delayed pulses originating from individual vertical sections arrive at the observer simultaneously.)

The map in Fig. 14 is supplemented by upper and lower frames demonstrating separately the waveforms at 100 and 1000 *km*. The lower frame illustrates that at short distance from the source each pulse is present in the field. The upper plot shows that at 1000 *km* distance the signal had already acquired the form of a single wave. Merging of sharp distinct initial pulses had completed at this distance. Two wide pulses left will unite at around 5000 *km* distance, as Fig. 13 shows.

We used for demonstrations the model of *negative* return stroke with equidistant partition. The reason is that the electric pulses from negative strokes are positive. Such excursions are much better recognized in the plots. It may be pointed out that contour maps of Figs. 13 and 14 will remain unchanged for positive strokes, only negative numbers should be placed at the scale bars.

In the previous section, we surveyed the results of analysis of electric fields in the vicinity of lightning stroke. We had shown that bent channels produce many pulses facilitating an initiation of non-linear effects. We had established before that a staircase channel may substantially enhance the ELF fraction in the discharge radiation. Here, we have indicated that individual pulses quickly merge into a single peak, and a remote observer cannot validate the nature of the source. Therefore, staircase discharges should be among probable candidates for the sources of the ELF transients associated with optical phenomena. The real strokes apparently have enhanced continuing current component, extended length and complicated geometrical structure of the channel combined from vertical and horizontal elements. Still our treatment demonstrated specific features arising from geometrical modifications.

6 Conclusion

Optical events over thunderstorms were successfully observed in different parts of the world[23,24]. The ground based observatories were placed at elevated sites located at a few hundred kilometers from the powerful night-time thunderstorms (MSCS). This allowed us to monitor the clear night sky above the thunderstorm cells with the top of clouds hidden by the horizon. Optical emissions are relatively weak and fast, therefore, a special equipment is used in such experiments[3, 4, 8, 7, 22]. To conduct such observations, one has to find a territory where MSCS are formed providing intense lightning activity at night, a remote elevated place to install optical equipment, and no optical sources along the line of vision, e.g., an unpopulated area.

A part of transient ELF signals originates from the same strokes that cause optical emissions in the middle atmosphere[8,21,22]. There is a hope that an ELF monitoring that allows establishing the coordinates of causative strokes will provide a statistical knowledge of the worldwide distribution of both optical events and MSCS. A typical ELF site must be placed far from industrial areas. The equipment contains a

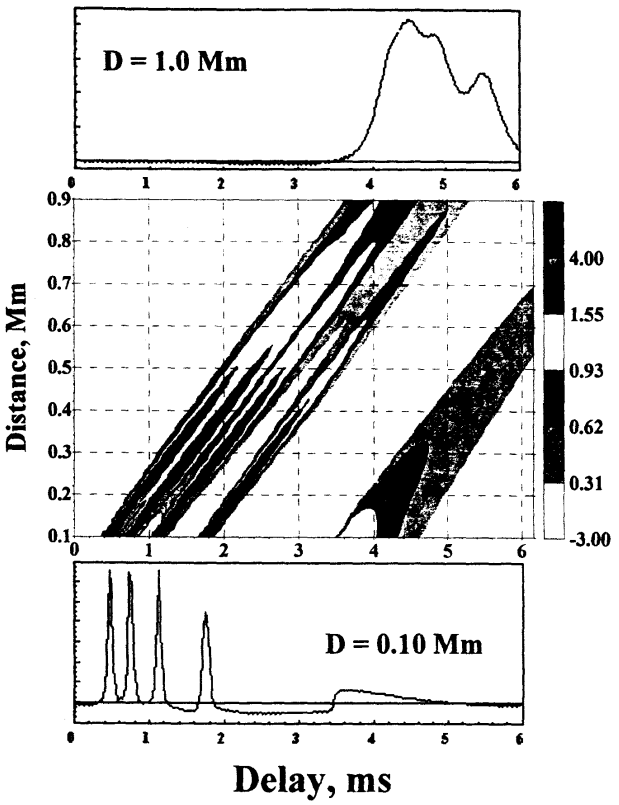

Fig. 14 Dynamics of ELF pulse from multiply bent the staircase stroke, in a close vicinity of the source. The upper and lower frames demonstrate separately the pulses at 100 and 1000 km distances. Four initiall pulses merge into single wave at 1000 km distance.

vertical electric and two perpendicular horizontal magnetic antennas, a receiver, ADC and computer collecting the data, and a timing system. A more detailed description of ELF measurements is found in the literature[8,9,16,17,20,21,25-27].

Only vertical strokes were used when modelling optical emissions and discrete ELF signals. We tried to demonstrate that modifications of the stroke geometry may produce substantial effects. Unfortunately, there are definite difficulties in an experimental validation of the above concept. Indeed, to detect multiple pulses in the vicinity of a bent stroke, one had to conduct the airborne measurements because many of these pulses vanish at the surface of conducting Earth. Multiple ELF pulses radiated by a vertical sections of staircase strokes rapidly merge into a single wave in the process of propagation. To detect such merging, one has to conduct simultan-eous observations at a system of sites equipped with standard wide-band ELF receivers, synchronized, and placed at different distances from the parent stroke.

We applied a typical model of the return stroke as the basic one and modified its geometry. We used idealized, strictly vertical and horizontal sections, the serial upward orientation of vertical sections. It is easy to introduce a stroke with a more sophisticated orientation of elements and conduct relevant computations. We did not concentrate on such adjustments, because they do not contribute into physical understanding, and simultaneously, the computed results loose their purity.

Geometry of the stroke and the progress of the current wave in the channel produce a variety of intense pulses that may advance the heating and breakdown effects. Joint impact of the static and transient fields helps initiate the plasma processes maintained afterwards by slowly decaying quasi-static field component. Transient electric fields scan the atmosphere, and random fluctuations of the electron collision frequency above the thunderstorm may govern the position and structure of optical phenomena.

Here we repeat the main results of the paper: Bending of the lightning channel expands the number radiated pulses. Vertical sections of a stroke are responsible for its quasi-static background field that exists until the charge dipole moment persists. The horizontal currents generate more intense pulses that contribute to the transient electric field in the atmosphere. Orientation of horizontal sections controls the magnitude and direction of transient electric fields in the mesosphere. It acquires vertical, horizontal radial and sideways components at the onset of each arriving pulse. The horizontal distance where the electron focusing may occur lies between 25 and 75 *km* from the stroke base. Branching of the stroke decreases the radiation from its horizontal currents due to interference between individual pulses. This is why the horizontal part of a symmetrical spider stroke does not radiate.

Most of the discrete pulses vanish at the ground surface or right above the stroke. Only airborne observations may disclose the above features. Distances of tens of kilometers from the discharge are appropriate and as high altitudes as possible.

Geometrical extension of a vertical discharge increases the ELF portion in its current moment. The

growth is directly proportional to the channel length. A plasma channel between ionosphere and the ground appears to be an excellent candidate for the causative strokes of ELF transients.

The ELF radiation of a bent stroke is associated solely with its vertical branch. The staircase geometry of the channel may enhance the ELF fields by an order in magnitude without any increase of the current or charge transfer. Frequency decay of the current moment in a model of staircase stroke agrees with the ELF experimental data deduced from the Q-bursts and slow tail atmospherics.

Multiple pulses from a staircase stroke turn into a single wave when propagating in the Earth ionosphere cavity. The transformation is complete at the source-observer distance greater than 5000 km. Therefore, a remote observer is not able to distinguish between the staircase and the vertical lightning discharges.

References

1 D D Sentman and E M Westcott *Geophys Res Lett* **20** (1993) 2857

2 E M Westcott, D D Sentman, D L Osborne, D L Hampton and M J Heavner *Geophys Res Lett* **22** (1995) 1209

3 W A Lyons *J Geophys Res* **101** (1996) 29 641

4 W A Lyons, M Uliasz and T E Nelson *Mon Weather Rev* **126** (1998) 2217

5 V P Pasko, U S Inan, Y N Taranenko and T F Bell *Geophys Res Lett* **22** (1995) 365

6 V P Pasko, U S Inan and T F Bell *Geophys Res Lett* **23** (1996) 301

7 C J Rodger *Rev Geophys* **37** (1999) 317

8 E Huang, E Williams, R Boldi, S Heckman, W Lyons, M Taylor, T Nelson and C Wong *J Geophys Res* **104** (1999) 16, 943

9 D Ll Jones *ELF Sferics and Lightning Effects on the Middle and Upper Atmosphere Modern Radio Science 1999*, (Ed by M A Stuchly) Published for URSI by Oxford Univ Press (1999) 171

10 A P Nickolaenko *Geomag and Aerono* **16** (1976) 260 (in Russian)

11 K I Kucherov and A P Nickolaenko *Izvestija vuzov Radiofizika* **22** (1979) 894 (in Russian)

12 A P Nickolaenko and M Hayakawa *Geophys Res Lett* **22** (1995) 3015

13 U S Inan, T F Bell and J V Rodriguez *Geophys Res Lett* **18** (1991) 705

14 Y N Taranenko, U S Inan and T F Bell *Geophys Res Lett* **20** (1993) 1539

15 E Williams *Science* **256** (1992) 1184

16 T Ogawa, Y Tanaka, A C Fraser-Smith and R Gendrin *J Geomag Geoelectr* **19** (1967) 377

17 D T Kemp and D Ll Jones *J Atmos Terr Phys* **33** (1971) 567

18 P V Bliokh, A P Nickolaenko and Yu F Filippov *Schumann Resonances in the Earth-Ionosphere Cavity* Peter Perigrinus London - New York (1980)

19 A P Nickolaenko and I G Kudinsteva *J Atmos Terr Phys* **56** (1994) 1493

20 C P Burke and D Ll Jones *J Atmos Terr Phys* **58** (1996) 531

21 D J Boccippio, E Williams, W A Lyons, I Baker and R Boldi *Science* **269** (1995) 1088

22 I H Marshall, L C Hale, C L Croskey and W A Lyons *J Atmos Solar-Terr Phys* **60** (1998) 77

23 R Dowden, S Hardman, J Brundell, J Bahr, Z Kawasaki and K Nomura *IEEE Ant Prop Mag* **39** (1997) 106

24 W A Lyons, T E Nelson, R A Armstrong, E R Williams, D M Susczysky, R Strabley, M Taylor and L Gardner *Proc 11th Interna Conf Atmosp Electricity Guntersville Alabama June 7-11 1999* Marshall Space Flight Center Alabama (1999) 84

25 G Satori, J Szendroi and J Vero *J Atmos Terr Phys* **58** (1996) 1475

26 A V Shvets *Radiofizika and Electronika* **2**(2) (1997) 101; Special Issue of *Jour of Atmosp Solar-Terrestrial Phys* **60**(7-9) (1998)

27 G G Beliajev, A Yu Schekotov, A V Shvets and A P Nickolaenko *J Atmos Solar-Terr Phys* **61** (1999) 751

28 D Ll Jones *J Atmos Terr Phys* **32** (1970) 1077

29 D R MacGorman and W D Rust *The Electrical Nature of Storms* Oxford University Press (1998)

30 T Ogawa Lightning Currents *Handbook of Atmospheric Electrodynamics* (**1**) (Ed H Volland) CRC Press Florida (1995) 93

31 M A Uman *The Lightning Discharge* Academic Press New York (1987)

32 C E R Bruce and R H Golde *J Inst Electr Eng* **88**(2) (1941) 487

33 V A Rakov *12-th International Zurich Symposium on Electromagnetic Compatibility* IEEE Switzerland Chapter on Electromagnetic Compatibility Zurich Switzerland Feb 16-18 1997

34 T Ogawa *J Geophys Res* **90** (1985) 5951

35 G Diendorfer and M A Uman *J Geophys Res* **95** (1990) 13, 621

36 A P Nickolaenko and M Hayakawa *J Geophys Res* **103-D** (1998a) 17 175

37 A P Nickolaenko and M Hayakawa *J Atmos Electr* **19** (1999a) 11

38 J R Wait *Electromagnetic Waves in Stratified Media* Pergamon Press New York London Toronto (1962)

39 J Galejs *Terrestrial Propagation of Long Electromagnetic Waves* Pergamon Press (1972)

40 V P Pasko, U S Inan, T F Bell and S C Reising *Geophys Res Lett* **25** (1998) 3493

41 T F Bell, S C Reising and U S Inan *Geophys Res Lett* **25** (1998) 1285

42 S A Cummer, U S Inan, T F Bell and Barrington-Leigh *Geophys Res Lett* **24** (1998) 1731

43 A P Nickolaenko and M Hayakawa *J Atmos Electr* **19** (1999b) 135

44 L C Hale *Adv Space Res* **4** (1984) 175

45 L C Hale *Proc 11th Intern Conf Atmos Electricity Guntersville Alabama June* 7-11 1999 Marshall Space Flight Center Alabama (1999) 151

46 U S Inan, W A Sampson and Y N Taranenko *Geophys Res Lett* **23** (1996) 133

47 A I Sukhorukov, E A Rudenchik and P Stubbe *XXVth General Assembly of URSI* Lille-France August 28 to September 5 (1996)

48 H L Rowland *J Atmos Solar-Terr Phys* **60** (1998) 831

49 M J Rycroft and M Cho *J Atmos Solar-Terr Phys* **60** (1998) 889

50 L C Hale and M E Baginski *Nature* **329** (1987) 329

51 M E Baginski and G W Jarriel Jr *J Electrostatics* **33** (1994) 87

52 P V Bliokh *Atmospheric and Ionospheric Electromagnetic Phenomena Associated with Earthquakes* (Ed. M Hayakawa) Terra Sci Pub Tokyo (1999) 829

53 O A Molchanov *J Atmos Electr* **19** (1999) 87

54 A P Nickolaenko, V A Rafalsky, A V Shvets and M Hayakawa *J Atmos Electr* **14** (1994) 97

55 A P Nickolaenko and M Hayakawa *J Atmos Electr* **18** (1998b) 95

56 P R Krehbiel, R J Thomas, W Rison, T Hamlin, J Harlin and M Davis *EOS Transactions AGU* **81**(3) (2000) 21